sustainable chemistry

MDPI

Article

A Sustainable Circular Route for PET LDH Nanocomposites: Catalyst-Driven Polymerization and Depolymerization for a BHET-to-BHET Cycle

Tsung-Yen Tsai [1,2,3,*], Basharat Hussain [1] and Naveen Bunekar [1]

[1] Department of Chemistry, Chung Yuan Christian University, 200 Chung Pei Road, Zhongli District, Taoyuan City 32023, Taiwan; basharathussain@cycu.org.tw (B.H.); naveen.bunekar@gmail.com (N.B.)
[2] Center for Nano-Technology, Chung Yuan Christian University, 200 Chung Pei Road, Zhongli District, Taoyuan City 32023, Taiwan
[3] R&D Center for Membrane Technology, Chung Yuan Christian University, 200 Chung Pei Road, Zhongli District, Taoyuan City 32023, Taiwan
* Correspondence: yen@cycu.edu.tw

Abstract

A sustainable circular pathway was developed for poly(ethylene terephthalate) (PET) nanocomposites through a catalyst-driven polymerization and depolymerization process. In this study, calcium dodecylbenzene sulfonate with n-butyl alcohol modified ZnAl layered double hydroxides (LDHs) were utilized as bifunctional catalysts to synthesize highly exfoliated PET/LDH nanocomposites via in situ polycondensation of bis(2-hydroxyethyl) terephthalate (BHET). The organic modification of LDHs expanded interlayer spacing, improved interfacial compatibility, and promoted uniform dispersion, leading to enhanced mechanical, thermal, and barrier properties. In the second stage, the pristine LDH catalyst efficiently depolymerized the prepared PET/LDH nanocomposites back into BHET through glycolysis, completing a closed-loop BHET-to-BHET cycle. This integrated strategy demonstrates the reversible catalytic functionality of LDHs in both polymerization and depolymerization, reducing metal contamination and energy demand. The proposed approach represents a sustainable route for designing recyclable high-performance PET nanocomposites aligned with the principles of green chemistry and circular material systems.

Keywords: closed-loop recycling; PET nanocomposites; LDH catalyst; sustainable chemistry; glycolysis depolymerization; circular polymer systems

Check for updates

Academic Editors: Carol López-de-Dicastillo, Eliezer Velásquez and Adrián Rojas Sepúlveda

Received: 27 November 2025
Revised: 6 January 2026
Accepted: 8 January 2026
Published: 16 January 2026

Copyright: © 2026 by the authors. Licensee MDPI, Basel, Switzerland. This article is an open access article distributed under the terms and conditions of the Creative Commons Attribution (CC BY) license.

1. Introduction

The development of sustainable polymer materials is essential to address global challenges such as plastic waste accumulation, resource depletion, and climate change. In line with the United Nations Sustainable Development Goals (SDGs), particularly SDG 12 (Responsible Consumption and Production), SDG 13 (Climate Action), and SDG 9 (Industry, Innovation and Infrastructure), there is a growing need to design high-performance polymers through environmentally friendly and resource-efficient methods. Sustainable synthesis of polymer nanocomposites provides a pathway to enhance material performance, reduce dependence on non-renewable resources, and minimize the environmental footprint of production. In this study, a sustainable strategy is proposed for developing high-performance PET nanocomposites using synthetic layered double hydroxides (LDHs)

as dual-function materials that serve as catalysts and reinforcing nanofillers during polymerization, and as catalysts for glycolysis-based depolymerization, thereby establishing a circular BHET-to-BHET pathway.

Poly(ethylene terephthalate) (PET) is among the most widely used polymers due to its excellent mechanical strength [1–4], chemical resistance [5–7], inherent recyclability [8–10], and ease of processability. However, its durability contributes to persistent plastic pollution, leading to the accumulation of micro- and nano-plastics in the environment [8–15]. To address this, polymer science increasingly emphasizes closed-loop systems that integrate synthesis, use, and recovery through sustainable catalytic design.

Nanocomposite technology contributes to sustainability by improving mechanical, thermal, and barrier properties, thus extending product lifetimes and reducing waste [16–19]. However, conventional clay-based fillers [20,21] are environmentally problematic due to open-pit mining [22–24], land degradation [25,26], biodiversity loss [27–30], soil erosion [31–33], and water pollution [34–36]. Their processing involves energy-intensive grinding, purification, and surface modification, significantly increasing the carbon footprint [37,38]. In contrast, synthetic LDHs, prepared from simple metal salts via low-temperature aqueous synthesis, offer a lower-carbon, mining-free alternative [39–42]. Proper exfoliation and homogeneous dispersion of LDH platelets play a key role in determining the final nanocomposite performance, as nanoparticle agglomeration can significantly deteriorate mechanical and barrier properties [43,44]. The well-dispersed and exfoliated structure obtained here minimizes such agglomeration effects, leading to notable improvements in modulus, tensile strength, thermal stability, and gas barrier behavior [45]. Owing to their brucite-like layered structure, expressed as $[M^{II}_{(1-x)}\, M^{III}_{x}\, (OH)_2]^{x+}(A^{n-})^{x/n}\cdot yH_2O$, allows controlled intercalation of anions for catalytic activity, capitalizing functions, while maintaining high purity and tunability [46–50].

In this work, calcium dodecylbenzene sulfonate with n-butyl alcohol (CDS) was intercalated into ZnAl-LDH to generate a bifunctional organophilic catalyst. The bulky surfactant increased interlayer spacing and compatibility with PET, enabling PET monomers to diffuse into the LDH galleries during in situ polymerization. This process promoted complete exfoliation and uniform LDH dispersion, forming PET LDH nanocomposites with superior mechanical strength, thermal stability, and gas barrier performance, achieved under mild, energy-efficient conditions consistent with green chemistry principles.

Despite advances in PET nanocomposites, their end-of-life management remains challenging. Mechanical recycling often leads to chain scission and performance loss, while chemical recycling through glycolysis provides a more sustainable route by depolymerizing PET into BHET [51]. Efficient glycolysis requires suitable catalysts to accelerate reaction rates and maximize BHET yield. Catalysts, including metal derivatives [52–54], ionic liquids [55], deep eutectic solvents [56], organic systems [57–59], and nano- catalysts such as metal oxides [60,61], metal nanoparticles [62], and LDHs [63–65], have been studied. LDHs are particularly attractive due to their dual acidic–basic sites, high reusability, and compositional tunability. For example, MgZnAl-LDHs achieved full PET conversion with a 75% BHET yield [66], Mg-Al hydrotalcite-type materials yielded 66.4% BHET at an Mg/Al = 3 ratio [67], ZnAl-CO_3 LDH produced a 79.3% yield, and ZnTi-LDH reached an 82% BHET yield with excellent recyclability [68,69]. These studies confirm LDHs as highly efficient, stable, and eco-friendly catalysts for PET glycolysis. Building upon this foundation, the present work introduces a closed-loop catalytic model uniting PET synthesis and chemical recycling within one framework. Modified LDHs serve as dual-function catalysts that promote in situ PET polymerization and later enable glycolytic depolymerization to regenerate BHET. In the first phase, organically modified LDHs catalyze polymerization and enhance filler dispersion, yielding reinforced PET nanocomposites. In the second phase,

pristine LDHs catalyze the reverse reaction, depolymerizing PET back to BHET monomers. This reversible transformation establishes a BHET-to-BHET circular cycle, eliminating toxic metal catalysts and reducing environmental waste. Overall, this study demonstrates a catalyst-driven circular pathway in which LDHs act as both catalytic and structural agents, achieving high-performance, recyclable PET nanocomposites aligned with sustainable and circular economy principles.

2. Materials and Methods

2.1. Materials

All chemicals and reagents used in this study were of analytical grade or the highest purity available, unless otherwise noted. Aluminum nitrate nonahydrate ($Al(NO_3)_3 \cdot 9H_2O$), Zinc nitrate hexahydrate ($Zn(NO_3)_2 \cdot 6H_2O$), sodium carbonate (Na_2CO_3), and sodium hydroxide (NaOH) were obtained from SHOWA Chemical Co. and Bis(2-hydroxyethyl) terephthalate (BHET) for catalyst premixing was sourced from Sigma-Aldrich (Merck KGaA, Darmstadt, Germany). BHET used as a raw PET monomer was provided by Shinkong Synthetic Fiber Corp. (Taipei, Taiwan). The surfactant calcium dodecylbenzene-sulphonate with n-butyl alcohol (together denoted CDS) were supplied by Taiwan Surfactant Corporation (Taipei, Taiwan). Ultrapure water (double-distilled) was produced by Cheer-Hsun Engineering Technology Co., Ltd. (Hsinchu County, Taiwan).

2.2. Synthysis of ZnAl LDH-CDS

ZnAl-LDH was synthesized via a hydrothermal co-precipitation method. Solution A was prepared by dissolving 8.42 g of $Zn(NO_3)_2 \cdot 6H_2O$ and 5.30 g of $Al(NO_3)_3 \cdot 9H_2O$ (Zn/Al molar ratio, 2:1) in 100 mL of deionized water. Solution B consisted of 6.04 g NaOH and 4.00 g Na_2CO_3 (NaOH/Na_2CO_3 molar ratio = 4:1), corresponding to concentrations of 1.5 M NaOH and 0.375 M Na_2CO_3, also dissolved in 100 mL of deionized water. Solution B was added dropwise to Solution A under vigorous stirring until the pH reached 10 ± 0.2. The resulting suspension was transferred to a Teflon-lined autoclave, made by Tung Kuang Glassware (Hsinchu, Taiwan) and hydrothermally treated at 150 °C for 12 h. After cooling to room temperature, the precipitate was collected by centrifugation, washed repeatedly with deionized water until neutral pH, freeze-dried, and ground to obtain pristine ZnAl-LDH. For organic modification, ZnAl-LDH was calcined at 600 °C for 1 h (heating rate: 5 °C min^{-1}) to form mixed metal oxides (MMO). One gram of MMO was dispersed in 50 mL of deionized water, and the pH was adjusted to 5 using dilute HNO_3. Subsequently, 1.17 g of organic modifier CDS was added gradually under continuous stirring. The mixture was hydrothermally treated at 150 °C for 12 h, followed by centrifugation, washing, freeze-drying, and grinding to obtain ZnAl LDH-CDS. This reconstruction intercalation route enables efficient surfactant incorporation under mild aqueous conditions, consistent with green chemistry principles.

2.3. Polymerization of PET ZnAl LDH-CDS Nanocomposites

BHET was used as the monomer for PET synthesis via melt polycondensation. A predetermined amount of BHET was charged into a reactor (Tung Kuang Glassware, Hsinchu, Taiwan) and melted at 245 °C under a nitrogen atmosphere to prevent oxidation and to remove residual moisture and ethylene glycol generated during the early stages of condensation. ZnAl LDH-CDS, pre-dried at 200 °C for 2 h to remove adsorbed moisture, was then introduced at loadings of 500, 800, and 1000 ppm relative to BHET. After homogeneous mixing, the temperature increased to 280 °C, and the system pressure was gradually reduced to below 1 torr to promote polycondensation. The reaction continued until the melt torque reached approximately 3 kgf·cm, indicating completion of polymerization. The

molten PET nanocomposites were extruded, quenched in chilled water, and pelletized. The resulting materials were denoted as PZD-500, PZD-800, and PZD-1000, corresponding to ZnAl LDH-CDS loadings of 500, 800, and 1000 ppm, respectively.

2.4. De-Polymerization of PET ZnAl-LDH-CDS Nanocomposites

To establish the closed-loop recyclability of the synthesized PET nanocomposites, a glycolysis reaction was employed to depolymerize the polymer matrix and recover its monomeric unit, BHET. PET nanocomposites (1.0 g, Figure 1a) were subjected to catalytic glycolysis using ZnAl-LDH as a heterogeneous catalyst. The reaction was performed in a 100 mL two-necked round-bottom flask containing 10 mL of EG and 0.01 g (1 wt.%) of ZnAl-LDH. The mixture was refluxed at 185 °C for 2 h under continuous stirring (400 rpm). After completion, the temperature was lowered to 100 °C to facilitate the separation of any unreacted PET. The heating was then discontinued, and the reaction was allowed to cool to approximately 65–75 °C. At this temperature, the reactor was opened, and the reaction mixture was visually inspected. In cases where a high yield was achieved, the reaction mixture appeared as a homogeneous brown suspension with the catalyst uniformly dispersed in a single-phase liquid (Figure 1b). The catalyst was removed by hot vacuum filtration, ensuring that the filtration apparatus was preheated to avoid premature precipitation of BHET and low-molecular-weight oligomers due to their temperature-dependent solubility in EG. The filtrate was then cooled to room temperature, where BHET and other oligomeric products gradually precipitated as a white solid (Figure 1c). The solid was further purified by pouring the reaction mixture into cold water and maintaining it at 4 °C overnight to allow complete crystallization of BHET. The resulting crystals were filtered and vacuum-dried at 65 °C to obtain the final white crystalline product (Figure 1d). The percentage yield of BHET was calculated according to the following expression:

$$\text{Yield BHET}(\%) = \frac{W_{rBHET}/MW_{BHET}}{W_{iPET}/MW_{PET}} \times 100\% \quad (1)$$

where W_{rBHET} and W_{iPET} are the weights of recovered BHET and initial PET, respectively, and MW_{BHET} and MW_{PET} are their respective molecular weight.

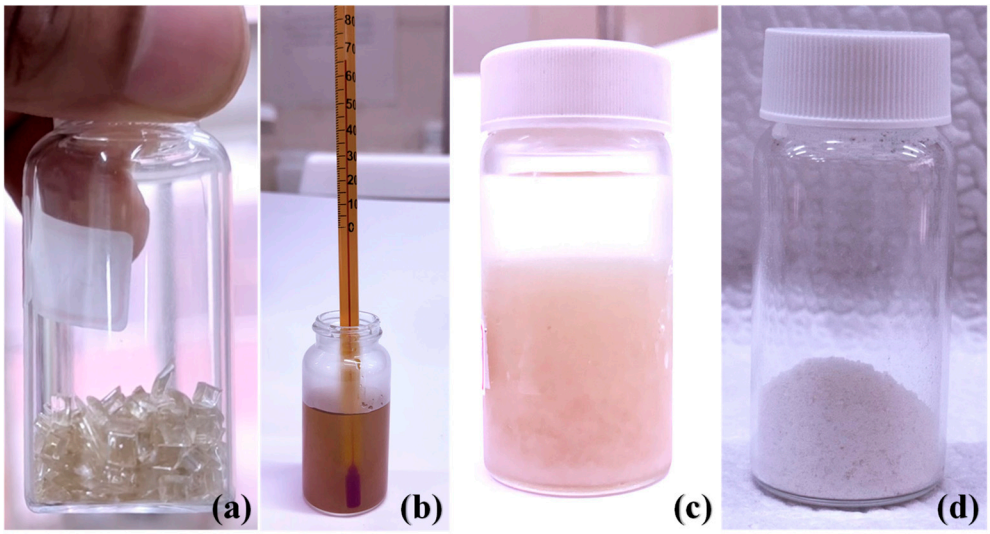


Figure 1. (**a**) PET Nanocomposites, (**b**) Reaction mixture of PET glycolysis at 65 °C containing the dispersed catalyst, (**c**) BHET crystals from recrystallization in cold water, and (**d**) Recovered BHET.

2.5. Characterization

The physicochemical properties of PET/MgAl-LDH-CDS nanocomposites were analyzed using various techniques. X-ray diffraction (XRD) was performed on a D8 Advance ECO (Bruker, AXS GmbH, Karlsruhe, Germany) using Cu Kα radiation (λ = 1.5406 Å, 40 kV, 25 mA) over a 2θ range of 2–80° with a step size of 0.05°. Fourier-transform infrared (FTIR) spectroscopy was carried out on a JASCO FTIR-4200 Type A (JASCO Inc., Tokyo, Japan) using KBr pellets (wavenumber range 400–4000 cm^{-1}). Morphology was examined by scanning electron microscopy (SEM, JEOL JSM-6500F (JEOL Ltd., Tokyo, Japan). Thermogravimetric analysis (TGA) was performed on an SII TG/DT analyzer (Nano Technology Inc., Tokyo, Japan) using 10 mg samples under nitrogen from 30 to 900 °C at a rate of 10 °C/min under nitrogen gas. DSC measurements were performed on a TA Q10 under nitrogen using heating-cooling-heating cycles from 30 to 280 °C at 10 °C min^{-1} (TA Instruments, New Castle, DE, USA). Gas permeability (GPA) was measured using a Yanco GTR-31 (GTR Tec Corporation, Kyoto, Japan). Dynamic mechanical analysis (DMA) was conducted on a TA-Q800 from 30 to 180 °C at 3 °C/min using film strips (10 × 5 × 0.03 mm^3). Optical properties were measured using a VARIAN Cary 100 UV-Vis spectrophotometer (Agilent Technologies, Santa Clara, CA, USA) in the wavelength range of 200–800 nm using free-standing films of uniform thickness. The viscosity-average molecular weight was determined using a Ubbelohde capillary viscometer (Cannon Instrument Co., Ubbelohde No. H531, State College, PA, USA) with 1,1,1,3,3,3-hexafluoro-2-propanol as the solvent at a polymer concentration of 0.5 mg mL^{-1} and calculated using the Mark-Houwink-Sakurada equation. Crystalline morphology was examined by polarizing optical microscopy (POM, LEICA DM 2500, Leica Microsystems, Wetzlar, Germany).

3. Result and Discussion

3.1. Structural Characterization of Modified ZnAl-LDH and ZnAl-LDH-CDS Nanocomposites

The XRD patterns of ZnAl LDH and modified ZnAl LDH are shown in Figure 2A(a,b), respectively. These patterns show the characteristic reflections of hydrotalcite-like structures of ZnAl LDH, with peaks at 2θ = 11.9° (d_{003}), 23.9° (d_{006}), 35.4° (d_{009}), 61.5° (d_{110}), and 62.9° (d_{113}). This result suggests that well-defined diffraction peaks with smooth baselines and sharp, narrow widths indicate the formation of a complete crystalline phase with high crystallinity. Furthermore, the $d_{(003)}$, $d_{(006)}$, and $d_{(009)}$ reflections exhibited a clear correlation, confirming the presence of an orderly and well-defined layered arrangement within the material's structure. The presence of reflections of (0012), (0015), (0018), (110) and (113) were indexed as the hexagonal lattice with rhombohedral 3R symmetry. The most intense peak in the XRD pattern corresponds to JCPDS card No. 38-0486, which is assigned to $Zn_6Al_2(OH)_{16}CO_3{\cdot}4H_2O$. This confirms that the synthesized ZnAl LDH exhibits characteristic diffraction patterns typical of layered double hydroxides. After modification with CDS, the XRD pattern of ZnAl LDH CDS (Figure 2A(b)) showed a marked reduction in peak intensity and a significant shift in the (003) reflection toward lower angles, appearing at 2θ, 2.98° (d_{003}, 29.6 Å). This pronounced expansion of the basal spacing confirms the successful intercalation of bulky dodecylbenzene sulphonate anions and carbon long chain of CDS into the interlayer galleries. The weakening and broadening of the higher-order reflections indicate partial loss of long-range ordering and increased disorder along the stacking direction, suggesting the disruption of the compact layered arrangement. Such structural modification aligns with the principles of sustainable chemistry, as it facilitates the development of highly dispersible and catalytically active LDH-based nanofillers, thereby enabling enhanced polymer-filler interactions while reducing the energy-intensive exfoliation steps in downstream processing.

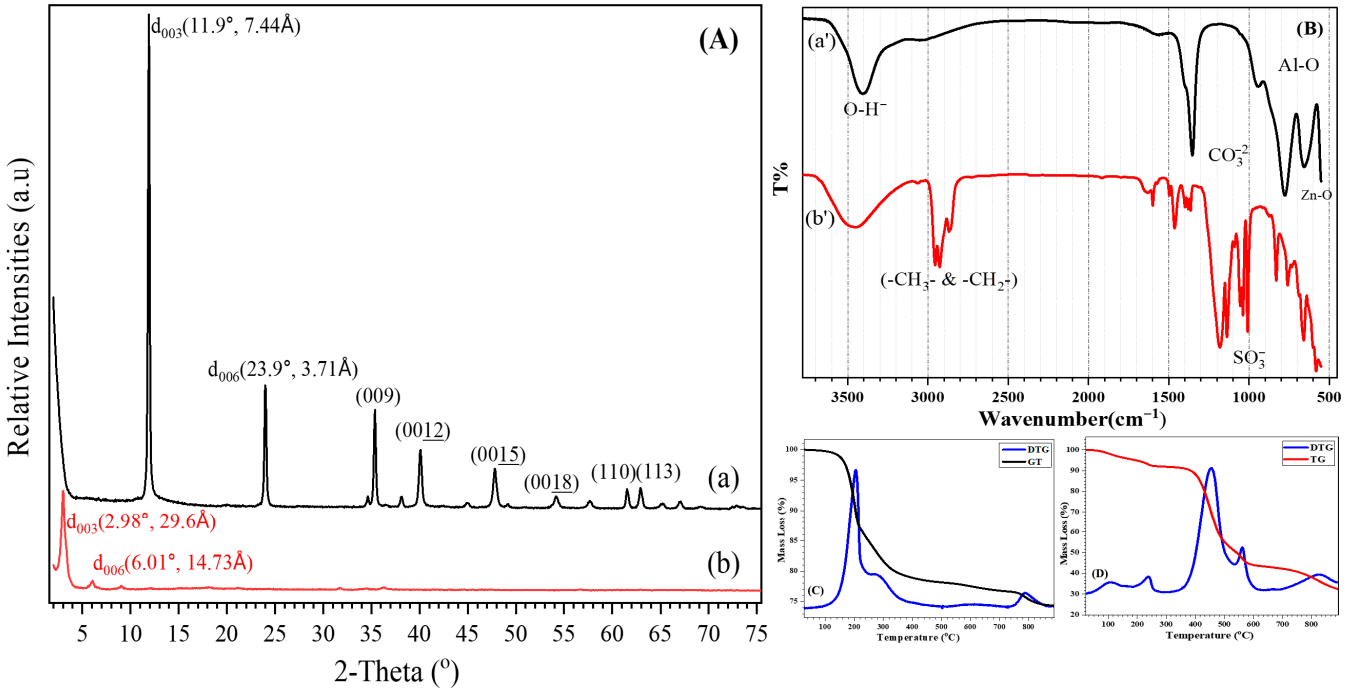


Figure 2. (**A**) XRD pattern (a) pristine ZnAl LDH, (b) ZnAl LDH-CDS, (**B**) FTIR spectra, (a′) pristine ZnAl LDH, (b′) ZnAl LDH-CDS, (**C**) TGA curves of pristine ZnAl LDH, (**D**) TGA curves of ZnAl LDH-CDS.

Following the confirmation of the crystalline structure and interlayer expansion by XRD analysis, SEM observations were conducted to further investigate the morphological changes induced by surfactant modification. As shown in Figure 3a, the pristine ZnAl LDH exhibited plate-like particles with well-defined hexagonal shapes and smooth surfaces. These particles appeared thicker and more compact, likely due to the larger ionic radius of Zn^{2+}, which enhances interlayer electrostatic interactions and promotes vertical crystal growth. Such structural order and high crystallinity suggest favorable properties for catalytic and reinforcement applications. In contrast, the morphology of the ZnAl LDH-CDS (Figure 3b) changed markedly after organic modification. ZnAl LDH-CDS showed loosely stacked platelets with opened and irregular edges, indicating successful intercalation of CDS molecules. The increased layer separation is consistent with the expanded basal spacing observed in the XRD patterns, confirming effective organic modification. In addition, the modified particles exhibited a more porous and fragmented structure, suggesting disruption of the original compact LDH architecture. The region highlighted by the red rectangle in Figure 3b was further magnified at a higher resolution (×50,000), as shown on the right, clearly revealing the thin, irregular morphology, indicating the breakdown of the original dense LDH framework along with noticeable distortion of their hexagonal geometry. This disruption is attributed to the dual role of CDS as both a dispersant and a spacing agent, which reduces interlayer cohesion and facilitates delamination of the LDH layers.

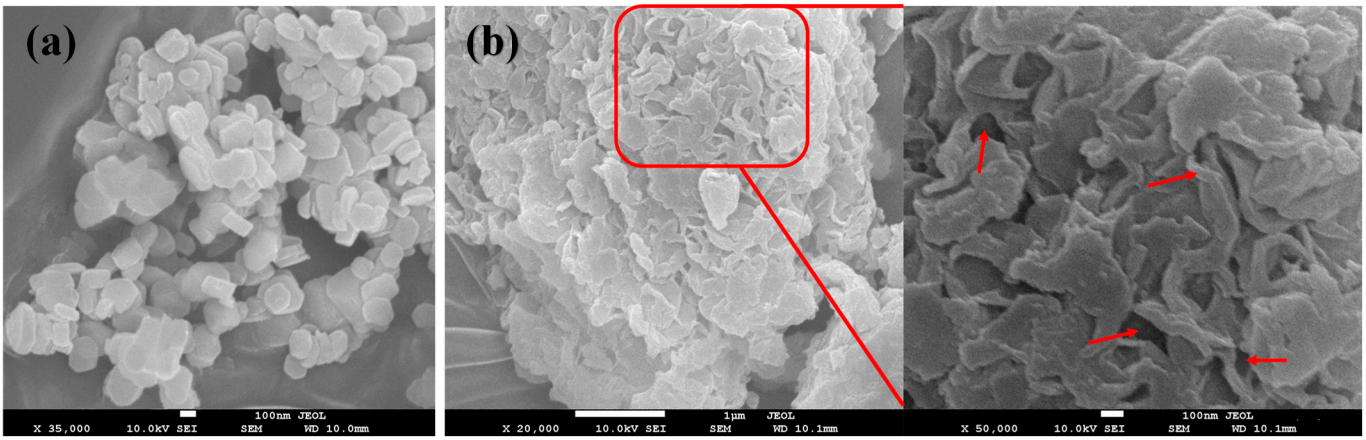


Figure 3. SEM micrographs of (**a**) pristine ZnAl LDH and (**b**) ZnAl LDH CDS.

Complementary to the structural information obtained from XRD and the morphological observations from SEM, FTIR spectroscopy was employed to examine the chemical functionalities of ZnAl LDH and to confirm the successful incorporation of surfactant species into the LDH structure. The FTIR spectrum of pristine ZnAl LDH Figure 2B(a′) shows a broad absorption band centered around 3450 cm^{-1}, corresponding to O-H stretching vibrations from hydroxyl groups in the brucite-like layers and interlayer water molecules.

A weak band near 1630 cm^{-1} is attributed to the bending vibration of interlayer water. The sharp band at approximately 1370 cm^{-1} is characteristic of the stretching vibration of interlayer carbonate (CO_3^{2-}) anions, while absorption bands below 800 cm^{-1} arise from metal oxygen lattice vibrations associated with Zn-O and Al-O bonds. After modification with CDS, the FTIR spectrum of ZnAl LDH-CDS Figure 2B(b′) exhibits several new features that confirm successful surfactant intercalation. Notably, the intensity of the carbonate band at 1370 cm^{-1} is significantly reduced, indicating effective replacement of CO_3^{2-} anions by CDS species within the LDH galleries. New absorption bands appearing at 2960, 2920, and 2850 cm^{-1} are assigned to the C-H stretching vibrations of -CH_2- and -CH_3 groups from the long alkyl chains of dodecylbenzene sulphonate. In addition, a strong band observed in the 1180–1040 cm^{-1} region corresponds to the symmetric and asymmetric stretching vibrations of sulfonate (SO_3^-) groups. The coexistence of these organic functional group signals with the characteristic LDH lattice vibrations confirms that the bulky DBSNBA anions were successfully incorporated into the interlayer galleries, leading to modified surface chemistry and enhanced organic compatibility of the LDH structure. TGA was performed to evaluate the thermal stability of pristine and modified ZnAl LDHs under conditions relevant to PET polymerization and depolymerization. The TGA curve of pristine ZnAl LDH (Figure 2C) shows three characteristic weight-loss stages. The first stage, up to approximately 250 °C (15.4%), corresponds to the removal of physically adsorbed and interlayer water. The second stage between 250 and 350 °C (6.3%) is attributed to the decomposition of interlayer carbonate species and partial dehydration. The final stage from 350 to 850 °C (4.9%) is associated with further dehydration and collapse of the brucite-like layers, leading to the formation of mixed metal oxides (ZnO-Al_2O_3). These results indicate that pristine ZnAl LDH is thermally stable up to ~250 °C, which is sufficient for the temperatures employed during PET glycolysis and catalyst pretreatment. In contrast, the modified ZnAl LDH–CDS (Figure 2D) exhibits a different thermal profile due to the presence of the intercalated organic surfactant. An initial weight loss of approximately 8.2% below 300 °C is attributed to the removal of free and interlayer water. A major decomposition step between 300 and 535 °C (55.6%) corresponds to the degradation of the aliphatic chains of CDS confined within the LDH galleries, followed by a minor loss

(3.6%) between 535 and 650 °C associated with the decomposition of aromatic components. The final stage up to 850 °C reflects the removal of residual anionic species and complete conversion to mixed metal oxides. The estimated organic loading (29.4 wt.%), calculated from the anion-exchange capacity, confirms effective intercalation of CDS, while the overall thermal behavior demonstrates that the modified LDH remains sufficiently stable within the temperature window relevant to PET processing and closed-loop recycling.

3.2. Structural and Thermal Stability Assessment of PET Nanocomposites

The XRD patterns of pristine PET and its nanocomposites containing 500, 800, and 1000 ppm of organo-modified LDHs are presented in Figure 4A. The semi-crystalline character of pristine PET was evidenced by a broad, amorphous region in its XRD pattern. In contrast, the characteristic (003) basal reflections of the modified LDHs were not detected in any of the PET LDH nanocomposites. This absence of LDH diffraction peaks suggests a loss of long-range crystalline order within the LDH phase, indicating that the layered structure was disrupted and exfoliated during in situ polymerization. The organic modifier CDS reduces the LDH surface hydrophobic, which promotes compatibility with the hydrophobic PET matrix and reduces electrostatic interactions between LDH platelets. This enhanced compatibility likely facilitates the penetration of PET chains into the interlayer galleries and promotes the delamination and exfoliation of LDH stacks, leading to highly dispersed nanofillers within the polymer matrix. Such exfoliated dispersion is a key strategy in sustainable nanocomposite design, as it maximizes surface contact and minimizes the amount of fillers required to achieve targeted property enhancements.

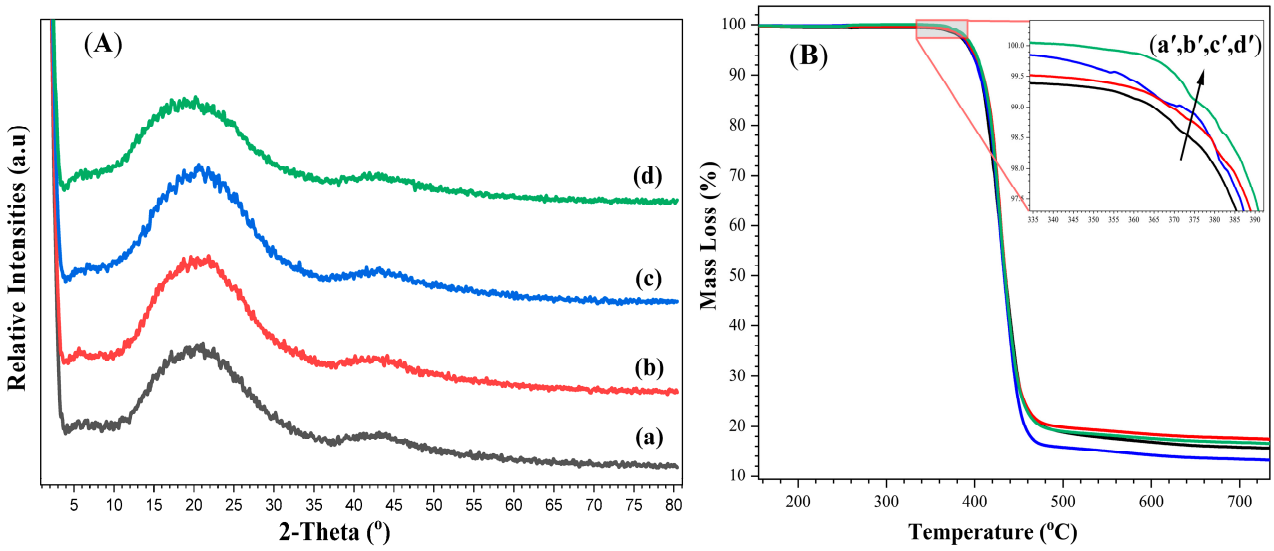


Figure 4. XRD patterns (**A**) of (a) Pristine PET, (b) PZD-500 ppm, (c) PZD-800 ppm, (d) PZD-1000 ppm nanocomposites, and TGA curves (**B**) of (a′) Pure PET (b′) PZD-500 ppm (c′) PZD-800 ppm (d′) PZD-1000 ppm nanocomposites.

TGA was employed to evaluate the thermal degradation behavior of neat PET and PET nanocomposites containing 500, 800, and 1000 ppm of modified LDHs Figure 4B. All samples exhibited a single main degradation step in the temperature range of approximately 350–470 °C, which is characteristic of PET thermal decomposition. Compared with pristine PET, the nanocomposites showed a slight shift in the degradation curves toward higher temperatures. The temperature at 5% weight loss (T_{5d}) increased by about 2.2, 3.1, and 5.2 °C for the 500, 800, and 1000 ppm samples, respectively. Considering the experimental uncertainty of TGA measurements (standard deviation ± 0.4 °C), these differences are modest and fall close to the normal error range of the technique. Therefore, the observed

changes should be interpreted as indicative trends rather than significant enhancements in thermal stability. The minor upward shift in T_{5d} may be related to the presence of well-dispersed LDH nanoplates, which can locally hinder heat transfer and slow the diffusion of volatile degradation products through a limited barrier effect. In addition, the organically modified LDHs may promote mild interfacial interactions with PET chains, resulting in a slightly more compact interphase. However, the overall degradation mechanism and thermal decomposition profile of PET remain essentially unchanged after LDH incorporation. Importantly, this study is not focused merely on thermal stability, it also addresses the simultaneous enhancement of mechanical and barrier properties, together with the demonstration of a closed-loop BHET to PET to BHET recycling process, achieved without compromising the sustainability of the overall system.

3.3. Crystallization Behavior of PET Nanocomposites

Figure 5A(a–d) presents the first-heating DSC thermograms of pristine PET and PET nanocomposites containing 500, 800, and 1000 ppm of ZnAl-LDH modified CDS, with the corresponding thermal parameters summarized in Table 1. The glass transition temperature (T_g) remains nearly unchanged for all samples, indicating that the incorporation of ultra-low loadings of modified LDHs does not significantly affect the segmental mobility of PET chains in the amorphous phase. During heating, the crystallization temperature (T_{ch}) shows only minor variations compared to neat PET, remaining in the range of 130 to 131 °C. This suggests that the presence of CDS-modified ZnAl-LDH has a limited influence on the onset of crystallization during heating and does not act as a strong nucleating agent under these conditions. The melting temperature (T_m), however, decreases gradually with increasing LDH content, with the most pronounced reduction observed at 1000 ppm. This melting point depression is attributed to the formation of thinner and less perfect lamellae, resulting from spatial confinement and interfacial interactions between PET chains and exfoliated LDH nanoplatelets decorated with long alkyl sulphonate chains. The DSC cooling curves (Figure 5B) reveal a clear shift in the crystallization temperature during cooling (T_{cc}) toward lower temperatures, decreasing from 197.9 °C for pristine PET to approximately 180 °C for all nanocomposites. This downward shift indicates a retardation of crystallization during cooling, rather than enhanced nucleation. The crystallization delay is associated with restricted chain diffusion and reduced molecular mobility caused by strong polymer filler interfacial interactions and steric hindrance introduced by the organically modified LDH layers. Although CDS modification improves LDH exfoliation and dispersion, the long alkyl chains promote adsorption of PET segments at the filler surface, which slows down crystal growth under non-isothermal cooling conditions. Despite the delayed crystallization during cooling, the degree of crystallinity (X_{ch}), calculated from the melting enthalpy, increases from 22.2% for neat PET to 26.6%, 27.5%, and 30.0% for PZD-500, PZD-800, and PZD-1000, respectively. This indicates that additional crystallization occurs during heating, where increased chain mobility enables PET segments previously constrained at the LDH interface to reorganize into more ordered crystalline structures. Such behavior is characteristic of polymer nanocomposites containing organically modified layered fillers, where crystallization kinetics are slowed during cooling, but the final crystallinity is enhanced upon thermal equilibration. Overall, the DSC results demonstrate that CDS-modified ZnAl-LDH does not function as a classical nucleating agent for PET but instead modulates crystallization behavior through interfacial confinement effects. Achieving higher crystallinity at ultra-low filler loadings ($\leq$0.1 wt.%) while maintaining simple processing aligns with the principles of sustainable polymer engineering.

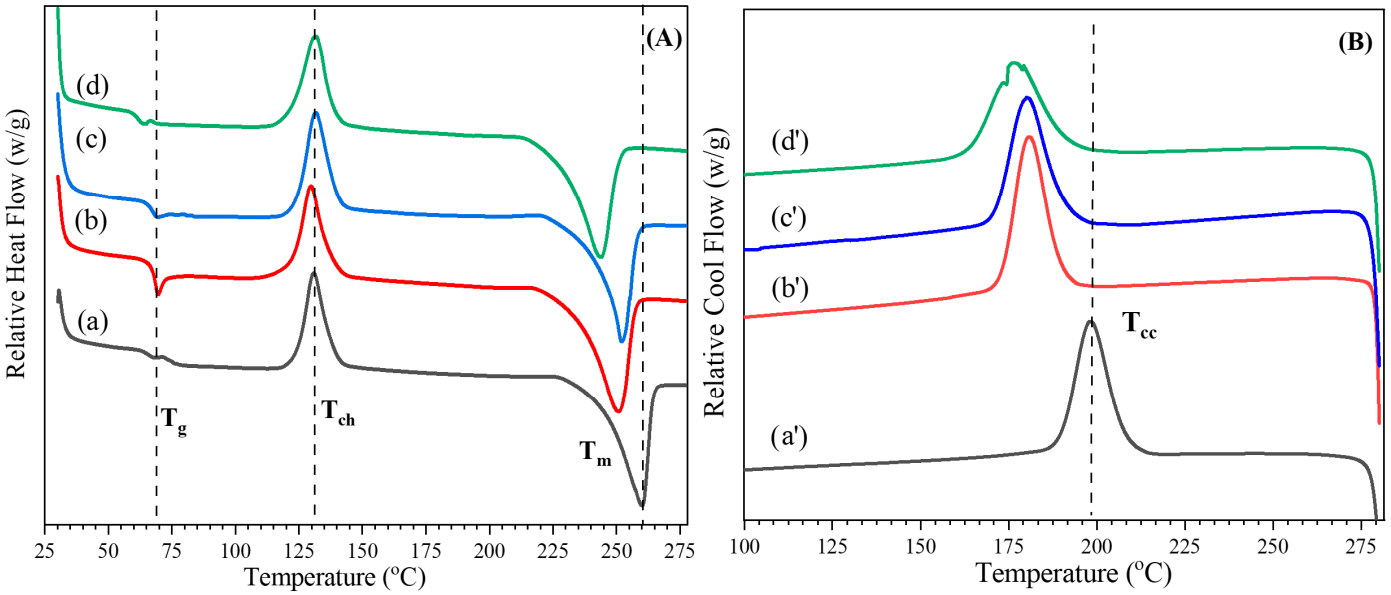


Figure 5. (**A**) DSC heating curve thermogram of pure PET and PET nanocomposites (a) pure PET (b) PZD 500 ppm (c) PZD 800 ppm (d) PZD 1000 ppm nanocomposites; (**B**) DSC cooling curve thermogram of pure PET and PET nanocomposites (a′) pure PET (b′) PZC 500 ppm (c′) PZC 800 ppm (d′) PZC 1000 ppm nanocomposites. The dashed vertical lines indicate T_g, T_{ch}, T_m and T_{cc}.

Table 1. DSC data of pure PET and PET composites (PZD) with different loadings of modified LDHs.

Samples	T_{ch} (°C)	T_{cc} (°C)	T_m (°C)	T_g (°C)	X_{ch} %
Pure PET	130.98	197.92	259.49	66.01	22.2
PZD-500	129.97	180.64	250.40	66.30	26.6
PZD-800	131.03	180.26	251.61	66.65	27.5
PZD-1000	131.67	180.64	243.48	65.12	30.0

3.4. Gas Barrier Properties of PET Nanocomposites

The oxygen transmission results of pristine PET and ZnAl LDH-CDS nanocomposites (PZD-500, PZD-800, and PZD-1000) are summarized in Table 2. Incorporation of organo-modified LDH platelets significantly reduced the oxygen permeability (O_2) of PET, with values decreasing from 0.6768 $cm^3 \cdot cm/(cm^2 \cdot s \cdot cm\text{-}Hg)$ for pure PET to 0.3381, 0.3164, and 0.2780 for PZD-500, PZD-800, and PZD-1000, respectively. The corresponding oxygen barrier improvement factors (O_2 BIF) increased progressively from 2.00 to 2.14 and 2.43, showing that the barrier performance was enhanced by up to 2.4-fold at just 1000 ppm of filler loading.

Table 2. Oxygen barrier properties of PET and PET nanocomposites.

Sample	Thickness (mm)	O_2 Barrer (cm^3 $cm/cm^2 \cdot s \cdot cm$-Hg)	O_2 BIF
Pure PET	0.19 ± 0.02	0.6768	-
PZD-500 ppm	0.17 ± 0.04	0.3381	2.00
PZD-800 ppm	0.18 ± 0.01	0.3164	2.14
PZD-1000 ppm	0.16 ± 0.02	0.2780	2.43

The marked reduction in oxygen permeability can be attributed to the uniform dispersion of the high aspect ratio modified LDHs platelets, which generate a tortuous diffusion pathway that forces gas molecules to travel around the impermeable nanolayers, thereby extending their permeation path and delaying transport through the polymer film. At the

same time, the improved interfacial adhesion between the organophilic LDH platelets and PET chains reduces micro voids that could otherwise serve as rapid diffusion channels. The incorporation of modified LDH also results in increased crystallinity and restricted segmental mobility of PET chains, leading to a stiffer and more tightly packed microstructure, which further hinders gas diffusion. The combined effects of physical reinforcement and microstructural ordering become more pronounced with increasing filler loading, with PZD-1000 showing the greatest improvement due to its denser and better-aligned nanoplatelet network. From a sustainable chemistry perspective, achieving substantial barrier enhancements at extremely low additive levels ($\leq$0.1 wt.%) reduces the material intensity and enables the production of thinner PET films without sacrificing performance. This not only decreases resource consumption and energy demand during processing but also extends the shelf life of packaged goods, reducing food and material waste. The synergy between low filler content, improved barrier efficiency, and enhanced durability demonstrates a resource-efficient route for developing high-performance PET-based packaging materials aligned with sustainable polymer engineering principles.

3.5. Insights from Polarizing Optical Microscopy (POM) into LDHs Dispersion and Intercalation with Organic Surfactants

The POM results provide direct visual evidence of the structure and property relationship governing the enhanced gas barrier performance of ZnAl LDH-CDS nanocomposites. The micrograph of pure PET (Figure 6a) shows a dark and nearly featureless field, confirming its highly amorphous structure where the polymer chains remain loosely packed and easily allow oxygen molecules to diffuse through the matrix. In contrast, the nanocomposites (Figure 6b–d) exhibit numerous bright birefringent crystalline domains, which increase in density and uniformity as the filler concentration rises. This progression clearly indicates that LDH platelets act as efficient heterogeneous nucleating agents, promoting the formation of more ordered regions that restrict segmental mobility and reduce free-volume pathways.

To complement the optical observations from POM, cross-sectional SEM imaging was performed on the 1000 ppm PET nanocomposite, where the higher filler content enables clear visualization of the actual fraction of dispersed single LDH platelets and their internal distribution within the matrix. As shown in Figure 6e, the film displays a homogeneous thickness of 434 μm with a compact and continuous microstructure, suggesting excellent processing stability and strong polymer filler compatibility. At higher magnification (Figure 6f), finely distributed LDH platelets can be distinguished throughout the matrix. The red-circled regions highlight nanoscale filler features rather than micro-scale tactoids, confirming effective dispersion and minimized aggregation. Moreover, the absence of crack deflection or platelet pull-out during fracture implies strong interfacial interaction, which contributes simultaneously to mechanical robustness and barrier reinforcement. Overall, the combined results of DSC, POM, and SEM establish a clear structure property relationship in which the synergistic increase in crystalline and nanoscale LDH dispersion creates a highly tortuous and extended diffusion pathway for gas molecules. Oxygen must navigate around impermeable crystalline zones and well-aligned LDH domains, significantly slowing its transport through the film. This mechanism explains the more than twofold reduction in oxygen permeability observed at 800–1000 ppm filler loading. Importantly, such substantial enhancement in barrier efficiency is achieved with $\leq$0.1 wt.% additive, enabling thinner PET packaging solutions without sacrificing performance. This reduction in polymer consumption supports sustainable material development by lowering environmental impact, extending product shelf life, and promoting circularity in packaging applications. Thus, the incorporation of ZnAl-LDH-CDS represents a promising low carbon strategy for producing high value, resource efficient PET nanocomposites.

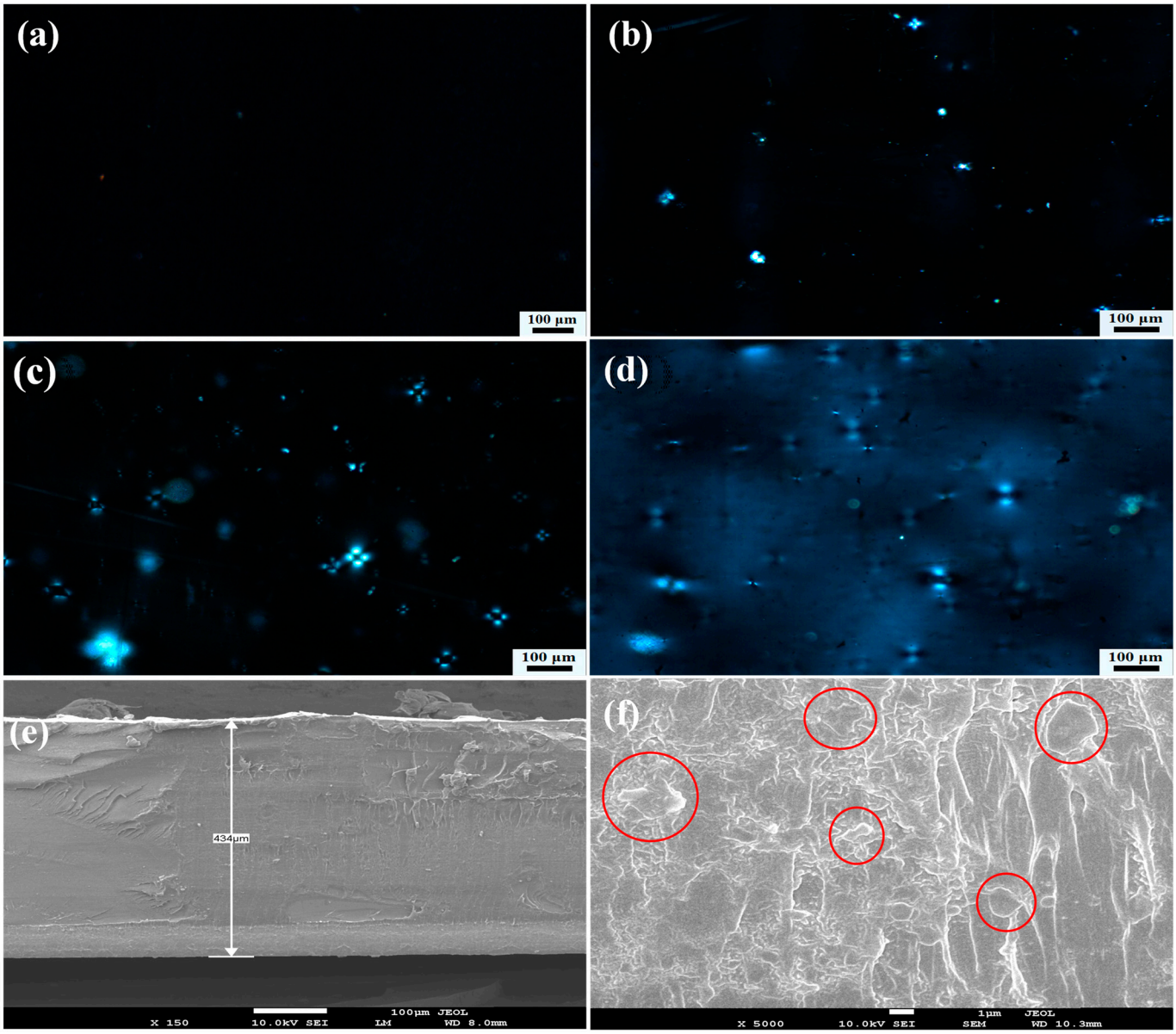


Figure 6. POM micrographs of pure PET and PET nanocomposites films (**a**) pure PET (**b**) PZD 500 ppm (**c**) PZD 800 ppm (**d**) PZD 1000 ppm and Cross-sectional SEM micrographs of PET nanocomposite films, (**e**) low-magnification (**f**) high-magnification. Red-circled regions indicate nanoscale filler features, suggesting good dispersion and minimal aggregation.

3.6. Optical Properties of Nanocomposites

The UV-Visible transmittance data of pristine PET and ZnAl LDH-CDS nanocomposites of PZD-500, PZD-800, and PZD-1000 are summarized in Table 3. Pristine PET showed high transmittance in the visible region (93.69% at 550 nm) but poor UV shielding, with 5.98% transmittance at 320 nm and 73.46% at 375 nm. Incorporation of ZnAl LDH-CDS significantly improved the UV-blocking ability without compromising visible transparency. The UV transmittance at 320 nm decreased progressively from 2.51% (PZD-500) to 3.73% (PZD-800) and as low as 0.59% for PZD-1000. A similar trend was observed at 375 nm, where transmittance decreased from 73.46% in pure PET to 42.13%, 61.11%, and 50.90% for PZC-500, PZC-800, and PZC-1000, respectively. Importantly, all nanocomposites maintained high visible light transmittance (>89% at 550 nm), confirming that the incorporation of LDH platelets does not compromise optical clarity.

Table 3. UV-Visible transmittance of pristine PET and PET nanocomposites.

Sample	Thickness (mm)	UV-Vis (nm) in % T		
		320 nm	375 nm	550 nm
Pure PET	0.22 ± 0.01	5.98	73.46	93.69
PZD-500 ppm	0.22 ± 0.02	2.51	42.13	89.81
PZD-800 ppm	0.21 ± 0.02	3.73	61.11	94.14
PZD-1000 ppm	0.22 ± 0.01	0.59	50.90	91.26

The improved UV shielding performance can be attributed to the strong UV absorption capability of the ZnAl LDH-CDS platelets and their uniform dispersion within the PET matrix, which enhances light scattering and creates a barrier to UV penetration. These platelets absorb and reflect UV radiation while preserving visible light transmission, resulting in a transparent yet UV-protective material. This synergistic combination of UV protection and optical clarity is especially valuable for applications in packaging and optical films, where photodegradation resistance is critical.

From a sustainable chemistry perspective, achieving strong UV shielding performance at extremely low additive loadings (≤0.1 wt.%) extends the service life of PET materials by minimizing UV-induced degradation and yellowing, reducing the frequency of material replacement and associated waste. By combining durability, clarity, and low material intensity, these PET/LDH nanocomposites exemplify resource-efficient, sustainable design for advanced packaging and engineering applications.

3.7. Mechanical Properties of the PET Nanocomposites

The influence of temperature on the storage modulus (E′) of pristine PET and PET ZnAl LDH–CDS nanocomposites is presented in Figure 7. The measurements were performed between 40 °C and 145 °C to evaluate their thermo-mechanical stability. In all samples, the storage modulus decreased progressively with increasing temperature, reflecting the enhanced molecular mobility of the polymer chains. As shown in Figure 7a–d, the storage modulus of the PET nanocomposites was consistently higher than that of pristine PET across the entire temperature range, demonstrating the reinforcing effect of the modified LDH platelets.

A sharp decline in E′ was observed between approximately 55 °C (glassy region) and 85 °C (rubbery region), which corresponds to the glass transition region of PET [70–72]. This transition is attributed to segmental chain relaxation, which reduces stiffness and storage modulus. Beyond 85 °C, a partial recovery of E′ occurred, typically associated with cold crystallization of PET. Notably, pristine PET showed an earlier and steeper drop in E′ compared to the nanocomposites, highlighting the improved thermal and mechanical performance imparted by the LDH fillers. In the glassy region, the tightly packed polymer chains are restricted by strong intermolecular interactions, giving rise to a high modulus. As temperature increases, these restrictions are relaxed, resulting in greater molecular mobility and lower stiffness. The incorporation of ZnAl LDH-CDS counteracts this softening by restricting chain movement and improving stress transfer across the polymer filler interface. Quantitatively, the storage modulus values of the PET nanocomposites exceeded those of pristine PET by 456 MPa (500 ppm), 519 MPa (800 ppm), and 579 MPa (1000 ppm). The 1000 ppm nanocomposite displayed the highest E′, confirming that increased LDH content enhances interfacial adhesion and mechanical reinforcement [73].

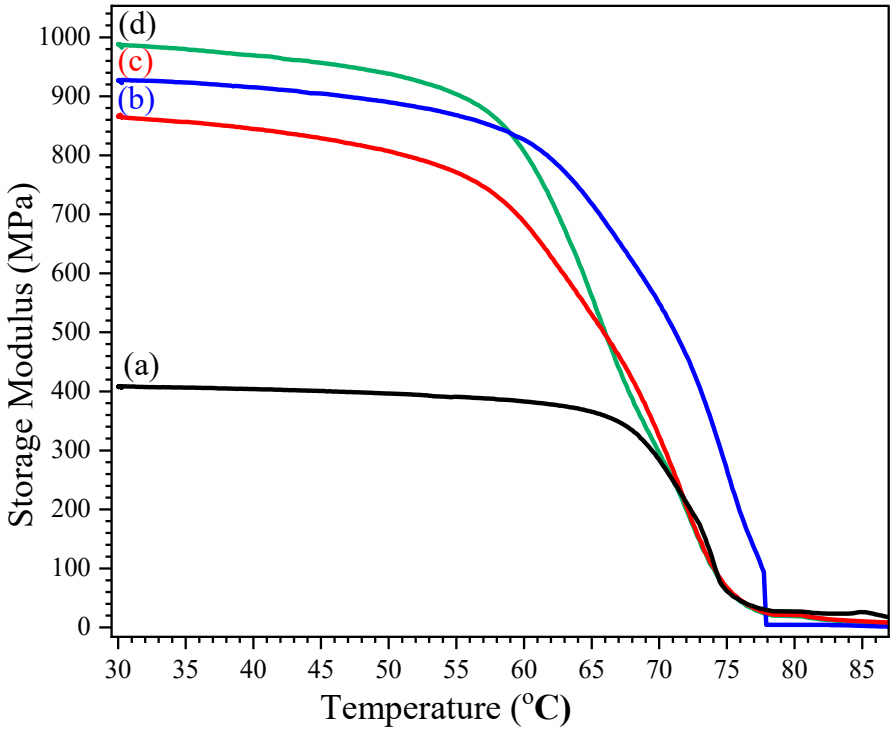


Figure 7. Storage modulus of (a) pure PET (b) PZD 500 ppm (c) PZD 800 ppm (d) PZD 1000 ppm nanocomposites.

3.8. Intrinsic Viscosity (IV) and Molecular Weight Determination of In-Situ Synthesized PET/LDH Nanocomposites

In line with the principles of sustainable polymer design, which aim to enhance material performance without increasing catalyst loading or processing complexity, the intrinsic viscosity (IV) and molecular weight of the in situ-synthesized PET nanocomposites were analyzed to examine how ZnAl LDH-CDS promotes chain growth and molecular build-up during polymerization.

Table 4 summarizes the intrinsic viscosity (IV) and molecular weight parameters of pristine PET and the in situ-synthesized ZnAl LDH-CDS nanocomposites. A distinct improvement in both the weight-average ($\overline{M}_w$) and number-average ($\overline{M}_n$) molecular weights is observed with the incorporation of the modified LDH, accompanied by higher IV values. Pristine PET exhibits an IV of 0.428 dL g^{-1} with $\overline{M}_w$ is 23,936 and $\overline{M}_n$ is 16,432. The nearly two-fold enhancement in molecular weight demonstrates that the ZnAl LDH-DBSNBA catalyst effectively promotes PET chain growth during the polycondensation process, indicating improved catalytic activity and polymer chain extension. The increase in molecular weight can be attributed to the catalytic effect of the ZnAl LDH layers, which provide abundant active sites that accelerate esterification and polycondensation reactions. The strong interfacial interactions between the organophilic LDH platelets and PET oligomers facilitate monomer adsorption and condensation at the LDH surface, leading to faster chain propagation and reduced chain termination. Additionally, the slightly higher Dispersity (Đ) values of the nanocomposites (1.5157–1.5267) compared to pristine PET (Đ 1.4567) indicate a broader molecular weight distribution typical of catalytically enhanced step-growth polymerization systems. The increase in storage modulus and the reduction in oxygen transmission rate (OTR) of the nanocomposites is attributed to the presence of well-dispersed CDS-modified ZnAl-LDH platelets, which reinforce the PET matrix by restricting segmental mobility and increasing crystallinity. In addition, plate like nanostructure introduces a tortuous diffusion pathway that hinders gas permeation, resulting in enhanced barrier performance. Intrinsic viscosity values confirmed that the nanocomposites possess a higher molecular

weight compared to pristine PET, indicating that polycondensation remains efficient in the presence of the modified LDH and that the mechanical and barrier improvements originate from structural reinforcement rather than polymer degradation. Achieving a substantial molecular weight increase at ≤0.1 wt.% filler highlights the catalytic efficiency of the ZnAl LDH-CDS system. This improvement enhances the mechanical strength, thermal stability, and long-term durability of PET nanocomposites. The approach exemplifies sustainable polymer design by reducing catalyst usage, energy demand, and material waste while maintaining high performance.

Table 4. Intrinsic Viscosity (IV) and Molecular Weight PET nanocomposites.

Samples	$\overline{M}_w$	$\overline{M}_n$	Đ	IV
Pure-PET	23,936	16,432	1.4567	0.428
PZD-500	42,739	28,198	1.5157	0.622
PZD-800	43,905	28,914	1.5185	0.633
PZD-1000	47,504	31,117	1.5267	0.666

3.9. Characterization of Recovered BHET and Its Role in Sustainable Circular Polymer Chemistry

The crystallized BHET obtained from the glycolysis of PET/LDH nanocomposites using pristine ZnAl LDH catalyst was analyzed by TGA, DSC, and ^{1}H NMR to verify its purity and recyclability within the circular PET system.

The TGA curve of the recovered BHET (Figure 8a) exhibits a clear two-step degradation behavior, with an initial weight loss around 212 °C attributed to the evaporation of residual ethylene glycol and low-molecular-weight BHET oligomers, followed by a major decomposition step near 412 °C corresponding to the breakdown of pure crystalline BHET. This two-stage pattern is characteristic of high-purity BHET and confirms the absence of polymeric residues. In comparison, the PET/LDH nanocomposites (Figure 4B(d′)) exhibit a single-step thermal degradation centered at approximately 400 °C, corresponding to the scission of the PET backbone and the formation of a minor inorganic residue from the LDH phase. The transition from a single-step polymer degradation in PET to a two-step profile in BHET provides strong evidence that the glycolysis reaction efficiently converted the PET/LDH nanocomposites into pure BHET monomer, thereby validating the success of the BHET to PET to BHET sustainable recycling loop.

The DSC thermogram (Figure 8b) reveals a single sharp melting endotherm at approximately 105.31 °C, which is consistent with the melting point of pure BHET. The narrow peak profile and absence of additional transitions suggest high crystallinity and homogeneity of the regenerated monomer. By contrast, the DSC curve of PET nanocomposites (Figure 5A(d)) exhibited glass-transition, cold-crystallization, and melting events typical of semicrystalline PET. These findings confirm that the glycolysis reaction effectively converted high-molecular-weight PET chains into uniform BHET crystals, supporting the principle of chemical circularity.

The ^{1}H NMR spectrum (Figure 8c) of the recovered BHET exhibits distinct signals confirming its molecular identity and purity. The resonance peak at δ 8.1 ppm corresponds to the four aromatic protons of the benzene ring, indicating the presence of the terephthalate moiety. The signals at δ 4.4 ppm and δ 3.9 ppm are assigned to the methylene protons adjacent to the ester (-CH_2OCO-) and hydroxyl (-CH_2OH) groups, respectively, verifying the intact glycol unit of BHET. Minor peaks from water at δ 3.3 ppm and DMSO-d_6 at δ 2.5 ppm are also present. The absence of any additional peaks from oligomeric or polymeric fragments confirms the complete depolymerization of PET and the successful regeneration of pure BHET suitable for depolymerization.

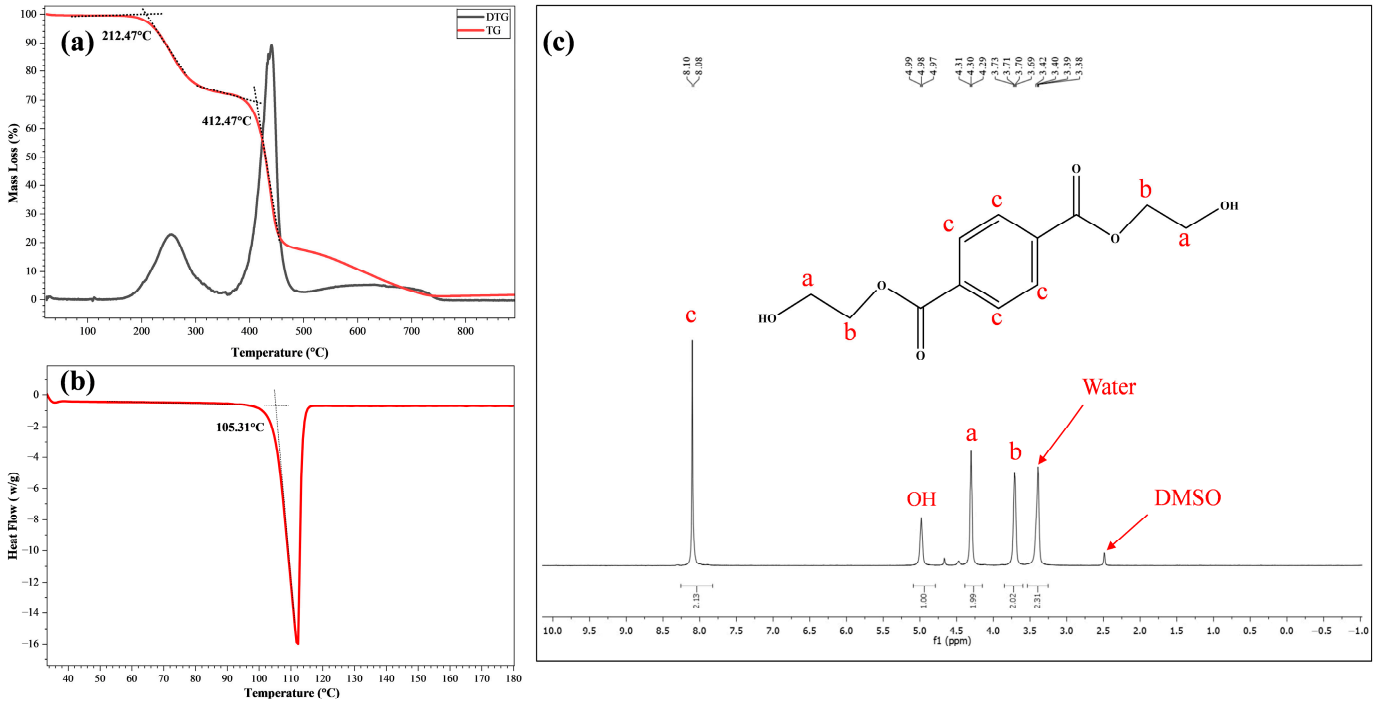
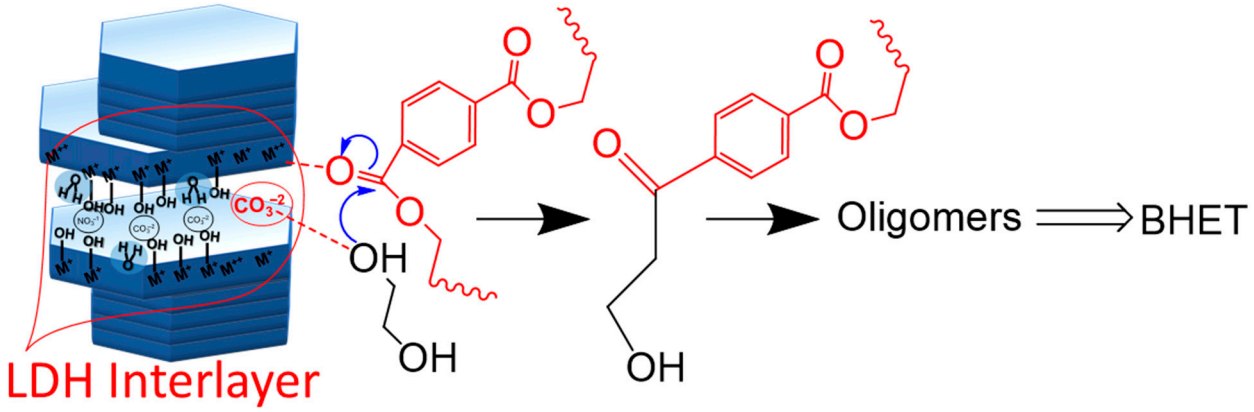


Figure 8. (**a**) TGA data of crystalized BHET, (**b**) DSC data of crystalized BHET, (**c**) ^{1}H NMR spectra data for crystallized BHET.

Collectively, these results demonstrate that ZnAl-LDH serves as an efficient and reusable catalyst for selective glycolytic cleavage of PET, leading to high-purity BHET with preserved molecular integrity. The identical thermal and spectroscopic characteristics of the regenerated BHET validate the sustainable chemical loop of BHET to PET to BHET, highlighting the potential of LDH-catalyzed systems to realize closed-loop, heavy-metal-free circular polymer chemistry in alignment with the goals of Sustainable Chemistry.

The glycolysis of PET begins when a deprotonated ethylene glycol molecule attacks the electron-deficient carbonyl carbon of the ester bond. An efficient catalyst must therefore increase the electrophilicity of this carbon while also promoting glycol deprotonation. In LDH-based catalysts, this occurs through the combined action of interlayer anions and surface hydroxyl groups. The metal cations in the LDH layer withdraw electrons from the carbonyl group, while the interlayer anions abstract protons from ethylene glycol to form the active glycolate species. When these anions are weakly bonded, proton abstraction is easier, leading to faster depolymerization. During glycolysis, ethylene glycol molecules can intercalate into the LDH galleries, enabling close interaction and efficient catalytic conversion of PET into BHET. A schematic representation of the proposed catalytic glycolysis mechanism is illustrated in Scheme 1.

This mechanism supports the BHET to PET to BHET circular process, where modified LDHs catalyze both polymerization and depolymerization under mild, low-energy conditions. Such a reversible, catalyst-driven cycle demonstrates the core principles of sustainable chemistry, including waste reduction, avoidance of heavy-metal catalysts, and enabling continuous material recovery within a closed-loop polymer system. The LDH layers effectively promoted ester bond cleavage during glycolysis, leading to complete depolymerization of PET. The glycolysis process effectively depolymerized the PET nanocomposites into high-purity BHET monomers, demonstrating complete (100%) conversion without leaving any unreacted polymer residue. The recovered BHET exhibited the same crystalline and structural characteristics as the original monomer, confirming the successful regeneration of feedstock suitable for repolymerization.



Scheme 1. Schematic representation of the proposed catalytic mechanism for PET depolymerization.

The yield of BHET was calculated according to the stoichiometric relation by Equation (1). Quantitatively, the overall BHET to PET to BHET recovery yield was approximately 77%, which should be regarded as a moderate value when considering both the polymerization and depolymerization steps. The yield loss can be attributed to the formation of low molecular weight oligomers (mainly dimers and trimers), as well as handling and purification losses, which are typical for laboratory scale glycolysis experiments. Nevertheless, the recovered BHET exhibited the same structural characteristics as the original monomer, indicating that the depolymerization process does not introduce chemical impurities that would hinder repolymerization. These findings demonstrate that the ZnAl LDH catalyst enables a simple and sustainable closed loop conversion between BHET and PET, while maintaining the monomer integrity necessary for repeat cycling. Although extended multi cycle evaluation is beyond the current scope, the results confirm the feasibility and recyclability potential of this catalyst assisted circular pathway within a resource efficient and low complexity process design.

In this study, CDS-modified ZnAl-LDH was incorporated into PET at $\leq$1000 ppm to act as a capitalizing and reinforcing nanofiller during polymerization. The long alkyl sulfonate chains reduce interlayer interactions and increase hydrophobicity, enabling exfoliation and strong interfacial contact with PET for improved dispersion and composite performance at ultralow additive levels. However, such concentrations do not provide enough catalytic sites for ester-bond cleavage. Therefore, unmodified ZnAl-LDH at 1 wt% was used as the glycolysis catalyst, where the Lewis-acidic Zn^{2+}/Al^{3+} centers and basic interlayer carbonate anions promote the nucleophilic attack of ethylene glycol necessary for PET depolymerization. Importantly, assigning two distinct yet complementary roles to the same LDH material modified for high performance polymer formation and unmodified for efficient BHET recovery enables a simplified, catalyst-compatible, and sustainable closed-loop recycling system. This approach reduces chemical consumption, avoids introducing foreign catalysts, and supports a resource-efficient circular-economy strategy for PET.

4. Conclusions

In this work, a sustainable circular route for poly(ethylene terephthalate) (PET) nanocomposites was successfully demonstrated through catalyst-driven polymerization and depolymerization, completing a reversible BHET-to-PET-to-BHET cycle. The bifunctional ZnAl-LDH catalyst, organically modified with calcium dodecylbenzene sulfonate with n-butyl alcohol, played a dual role in promoting polymerization and reinforcing the PET matrix. The organic modification expanded the LDH interlayer spacing and enhanced interfacial compatibility, leading to highly exfoliated PET/LDH nanocomposites with markedly improved properties. The crystallinity of the composites increased significantly,

accompanied by a barrier improvement factor (BIF) of 2.43, optical transparency above 90% at 550 nm, and UV shielding of about 50% at 375 nm. The incorporation of modified ZnAl LDH markedly enhanced PET performance, increasing its modulus from 23,936 MPa to 47,504 MPa, and its weight-average molecular weight ($\overline{M}_w$) from 23,936 g mol^{-1} to 47,504 g mol^{-1}, confirming the strong reinforcement achieved through uniform LDH dispersion. In the depolymerization, pristine ZnAl-LDH acted as an efficient heterogeneous catalyst for PET glycolysis, achieving complete polymer conversion and recovering BHET with a moderate yield (~77%). Although higher BHET yields have been reported using more complex catalytic systems, the present approach prioritizes process simplicity and sustainability by employing a single LDH-based catalyst without additional reagents. Structural analysis confirmed that the recovered BHET retained characteristics suitable for repolymerization, supporting the feasibility of closed-loop recycling. Overall, the results demonstrate that organically modified LDHs can serve as multifunctional additives for PET nanocomposites, enabling balanced improvements in structure, performance, and recyclability while adhering to the principles of sustainable and resource-efficient polymer engineering.

Author Contributions: Conceptualization, T.-Y.T. and B.H.; methodology, B.H. and N.B.; software, B.H.; validation, B.H., N.B. and T.-Y.T.; formal analysis, B.H. and N.B.; investigation, B.H., N.B. and T.-Y.T.; resources, T.-Y.T., B.H. and N.B.; data curation, B.H. and N.B.; writing—original draft preparation, B.H. and N.B.; writing—review and editing, T.-Y.T., B.H. and N.B.; visualization, B.H., N.B. and T.-Y.T.; supervision, T.-Y.T.; project administration, T.-Y.T.; funding acquisition, T.-Y.T. All authors have read and agreed to the published version of the manuscript.

Funding: We are grateful to the National Science & Technology Council on the Project "Study on the mechanism of preparation of polyester nanocomposites and recycling by chemical degradation using new catalysts" (NSTC 114-2635-M-033-001-MY3) for providing financial support for this research.

Data Availability Statement: The data supporting this study's findings are available upon request from the authors.

Acknowledgments: We are grateful to Chung Yuan Christian University, Department of Chemistry, Center for Nano-Technology and R&D Centre for Membrane Technology for providing all facility support for this work.

Conflicts of Interest: The authors declare no conflict of interest.

Abbreviations

The following abbreviations are used in this manuscript:

SDGs	Sustainable Development Goals
LDH	Layered Double Hydroxide
CDS	calcium dodecylbenzene sulphonate, n-butyl alcohol
BHET	Bis(2-hydroxyethyl) terephthalate
MMO	Mixed metal oxide
PET	Polyethylene terephthalate
XRD	X-ray diffraction
FTIR	Fourier transform infrared spectroscopy
SEM	scanning electron microscope
TGA	Thermogravimetric analysis
BIF	Barrier improvement factor
IV	Intrinsic viscosity
Đ	Dispersity
$\overline{M}_w$	Weight-average molecular weight
$\overline{M}_n$	Number-average molecular weight

References

1. El Darai, T.; Ter-Halle, A.; Blanzat, M.; Despras, G.; Sartor, V.; Bordeau, G.; Lattes, A.; Franceschi, S.; Cassel, S.; Chouini-Lalanne, N.; et al. Chemical recycling of polyester textile wastes: Shifting towards sustainability. *Green Chem.* **2024**, *26*, 6857–6885. [CrossRef]
2. Jexembayeva, A.; Konkanov, M.; Aruova, L.; Kirgizbayev, A.; Zhaksylykova, L. Modifying bitumen with recycled PET plastics to enhance its water resistance and strength characteristics. *Polymers* **2024**, *16*, 3300. [CrossRef] [PubMed]
3. Zahid, M.; Abbas, Y.M.; Shafiq, N.; Khan, M.I.; Ismail, F.I. Sustainable engineered geopolymer composites utilizing gamma-irradiated PET and graphene nanoplatelets: Optimization and performance enhancement. *Sustainability* **2024**, *16*, 7455. [CrossRef]
4. Steimel, K.G.; Hwang, R.; Dinh, D.; Donnell, M.T.; More, S.; Fung, E. Evaluation of chemicals leached from PET and recycled PET containers into beverages. *Rev. Environ. Health* **2024**, *39*, 251–260. [CrossRef] [PubMed]
5. Guo, Z.; Wu, J.; Wang, J. Chemical degradation and recycling of polyethylene terephthalate (PET): A review. *RSC Sustain.* **2025**, *3*, 2111–2133. [CrossRef]
6. Wang, Y.; Park, B.S.; Vu, V.P.; Lee, S.H. Self-healing conducting composite electrodes derived from chemical recycling of PET plastic wastes for flexible supercapacitors. *Polym. Eng. Sci.* **2025**, *65*, 1854–1867. [CrossRef]
7. Oyewale, J.A.; Tartibu, L.K.; Okokpujie, I.P. Decision analysis approaches on the collection methods of polyethylene terephthalate waste. *Recycling* **2024**, *9*, 124. [CrossRef]
8. Duan, C.; Wang, Z.; Zhou, B.; Yao, X. Global polyethylene terephthalate (PET) plastic supply chain resource metabolism efficiency and carbon emissions co-reduction strategies. *Sustainability* **2024**, *16*, 3926. [CrossRef]
9. Bharadwaj, C.; Purbey, R.; Bora, D.; Chetia, P.; R, U.M.; Duarah, R.; Dutta, K.; Sadiku, E.R.; Varaprasad, K.; Jayaramudu, J. A review on sustainable PET recycling: Strategies and trends. *Mater. Today Sustain.* **2024**, *27*, 100936. [CrossRef]
10. Enache, A.C.; Grecu, I.; Samoila, P. Polyethylene terephthalate (PET) recycled by catalytic glycolysis: A bridge toward circular economy principles. *Materials* **2024**, *17*, 2991. [CrossRef]
11. Hossain, M.T.; Shahid, M.A.; Mahmud, N.; Darda, M.A.; Samad, A.B. Techniques, applications, and prospects of recycled polyethylene terephthalate bottle: A review. *J. Thermoplast. Compos. Mater.* **2024**, *37*, 1268–1286. [CrossRef]
12. Gracida-Alvarez, U.R.; Xu, H.; Benavides, P.T.; Wang, M.; Hawkins, T.R. Circular economy sustainability analysis framework for plastics: Application for poly(ethylene terephthalate) (PET). *ACS Sustain. Chem. Eng.* **2023**, *11*, 514–524. [CrossRef]
13. Shi, X.; Chen, Z.; Wei, W.; Ni, B.J. Perspectives on sustainable plastic treatment: A shift from linear to circular economy. *TrAC Trends Anal. Chem.* **2024**, *173*, 117631. [CrossRef]
14. Caelli, C.; Arfelli, F.; Caraceni, F.; Cespi, D.; Cordara, M.; Brondi, C.; Ballarino, A. Implementation of LCA in the circular economy context: Methodological issues for application in PET packaging. *Procedia CIRP* **2024**, *122*, 719–724. [CrossRef]
15. Jürgens, M.; Endres, H.J. Environmental impacts of circular economy practices for plastic products in Europe: Learnings from life cycle assessment studies. *Procedia CIRP* **2024**, *122*, 312–317. [CrossRef]
16. Rajeshkumar, G.; Seshadri, S.A.; Ramakrishnan, S.; Sanjay, M.R.; Siengchin, S.; Nagaraja, K.C. A comprehensive review on natural fiber/nano-clay reinforced hybrid polymeric composites. *Polym. Compos.* **2021**, *42*, 3687–3701. [CrossRef]
17. Meri, R.M.; Zicans, J.; Maksimovs, R.; Ivanova, T.; Kalnins, M.; Berzina, R.; Japins, G. Elasticity and long-term behavior of recycled polyethylene terephthalate (rPET)/montmorillonite composites. *Compos. Struct.* **2014**, *111*, 453–458. [CrossRef]
18. Marzuki, N.H.; Irfiani, N.; Wahit, M.U.; Othman, N.; Yusoff, N.I.S. Mechanical properties of kenaf fiber and montmorillonite reinforced recycled polyethylene terephthalate/recycled polypropylene. *Mater. Today Proc.* **2018**, *5*, 21879–21887. [CrossRef]
19. Abulyazied, D.E.; Ene, A.; Bashir, Z.; Al-Zahrani, S.M. An investigative study on nanoclay-reinforced polymers: Preparation, properties, and applications. *Polymers* **2021**, *13*, 4401. [CrossRef]
20. Taha, Z.T.; Bata, A.; Molnár, B.; Ronkay, F. Impact of montmorillonite reinforcement on the recyclability of bio- and petroleum-based polyesters. *Heliyon* **2025**, *11*, e43022. [CrossRef]
21. Chandra, A.; Siddiqua, S. Sustainable utilization of chemically depolymerized polyethylene terephthalate (PET) waste to enhance sand–bentonite clay liners. *Waste Manag.* **2023**, *166*, 346–359. [CrossRef] [PubMed]
22. Mirzehi, M.; Afrapoli, A.M. Sustainable long-term production planning of open-pit mines: An integrated framework for concurrent economical and environmental optimization. *Resour. Policy* **2024**, *94*, 105131. [CrossRef]
23. Qi, X.; Zhou, W.; Li, R.; Tian, Y.; Lu, X. Study on the development rule of mudstone cracks in open-pit mine dumps improved with xanthan gum. *Appl. Sci.* **2024**, *14*, 10194. [CrossRef]
24. Wang, Z.; Yang, T.; Liu, Y.; Jiang, Q.; Shang, H.; Zheng, C. Montmorillonite combined with microbially induced carbonate precipitation for wind erosion control of bare surface soil in arid mining area. *Process Saf. Environ. Prot.* **2024**, *187*, 926–939. [CrossRef]
25. He, Y.; Lai, Y.; Chen, B.; Chen, Y.; Xie, Z.; Yu, X.; Luo, M. An open-pit mines land-use classification method based on random forest using UAV: A case study of a ceramic clay mine. *Minerals* **2024**, *14*, 1282. [CrossRef]

26. Ramly, N.A.; Hendraningrat, L.; Riyanto, L.; Shafie, N.A.; Piah, M.F.M.; Borhan, N. A clay stabilizer technology replication for production enhancement in a brown field. In Proceedings of the International Petroleum Technology Conference, Kuala Lumpur, Malaysia, 18–20 February 2025. [CrossRef]
27. Haq, I.U.; Elahi, A.; Khan, A.; Ali, A.; Qureshi, Q.B.A.I.L.; Rezzoug, A.; Mumtaz, M.A. The addition of natural clay and industrial and agricultural waste on the performance of green and sustainable concrete. *Sci. Rep.* **2025**, *15*, 823–838. [CrossRef]
28. Almeida, J.L. Environmental impacts caused by clay extraction in the municipality of Ibiassucê-BA. *Rev. Cient. Multidiscip. Núcleo Conhecimento* **2020**, *3*, 35–46. [CrossRef]
29. Robinson, J.M.; Liddicoat, C.; Muñoz-Rojas, M.; Breed, M.F. Restoring soil biodiversity. *Curr. Biol.* **2024**, *34*, R393–R398. [CrossRef]
30. Ding, J.; Eldridge, D. Intensifying aridity induces tradeoffs among biodiversity and ecosystem services supported by trees. *Glob. Ecol. Biogeogr.* **2024**, *33*, e13894. [CrossRef]
31. Musa, O.; Samuel, J.O.; Adams, M.; Abdulsalam, M.; Nathaniel, V.; Maude, A.M.; Adedayo, O.A.; Tiamiyu, A.G.T. Soil erosion, mineral depletion and regeneration. In *Prospects for Soil Regeneration and Its Impact on Environmental Protection*; Springer: Berlin/Heidelberg, Germany, 2024; pp. 159–172. [CrossRef]
32. Ayoubi, S.; Milikian, A.; Mosaddeghi, M.R.; Zeraatpisheh, M.; Zhao, S. Impacts of clay content and type on shear strength and splash erosion of clay–sand mixtures. *Minerals* **2022**, *12*, 1339. [CrossRef]
33. Attom, M.F.; Milikian, A.; Mosaddeghi, M.R.; Zeraatpisheh, M.; Zhao, S. Prediction of internal erosion parameters of clay soils using initial physical properties. *Water* **2024**, *16*, 232. [CrossRef]
34. Qi, J.; Yu, J.; Shah, K.J.; Shah, D.D.; You, Z. Applicability of clay/organic clay to environmental pollutants: Green way—An overview. *Appl. Sci.* **2023**, *13*, 9395. [CrossRef]
35. Anju, P.S.; Jaya, D.S. Impacts of clay mining activities on aquatic ecosystems: A critical review. *Int. J. Eng. Adv. Technol.* **2022**, *11*, 128–134. [CrossRef]
36. Waleed, M.H.; Khan, W. Water pollution and its control through adsorbents of clay-based materials. *J. Wastes Biomass Manag.* **2024**, *6*, 1–10. [CrossRef]
37. Hernández García, L.C.; Monteiro, S.N.; Lopera, H.A.C. Recycling clay waste from excavation, demolition, and construction: Trends and challenges. *Sustainability* **2024**, *16*, 6265. [CrossRef]
38. Quinteiro, P.; Araújo, A.; Oliveira, B.; Dias, A.C.; Arroja, L. The carbon footprint and energy consumption of a commercially produced earthenware ceramic piece. *J. Eur. Ceram. Soc.* **2012**, *32*, 2087–2094. [CrossRef]
39. Sharma, R.; Arizaga, G.G.C.; Saini, A.K.; Shandilya, P. Layered double hydroxide as multifunctional materials for environmental remediation. *Sustain. Mater. Technol.* **2021**, *29*, e00319. [CrossRef]
40. Altalhi, A.A.; Mohamed, E.A.; Negm, N.A. Recent advances in layered double hydroxide (LDH)-based materials. *Energy Adv.* **2024**, *3*, 2136–2151. [CrossRef]
41. He, X.; Yang, J.; Niu, M.; Han, A.; Li, G. Synthesis of CaLiAl-LDHs and optimization on chloride binding in marine cement materials. *J. Clean. Prod.* **2024**, *443*, 141183. [CrossRef]
42. Bai, C.; Luo, Q.; Zhang, H.; Dong, M.; Li, J.; Wang, X.; Li, M.; Ma, F.; Wu, Z.; Du, X. Low-temperature one-pot synthesis of Fe-doped hydrotalcite for enhanced boron adsorption. *Desalination* **2025**, *597*, 118391. [CrossRef]
43. Zeinedini, A.; Akhavan-Safar, A.; da Silva, L.F.M. The role of agglomeration in the physical properties of CNTs/polymer nanocomposites: A literature review. *J. Mater. Des. Appl.* **2025**, 1–39. [CrossRef]
44. Zare, Y. Study of nanoparticles aggregation in polymer particulate nanocomposites by mechanical properties. *Compos. Part A* **2016**, *84*, 158–164. [CrossRef]
45. Naveen Kumar, M.; Kumar, K.R.V.; Suresh, G.; Muthukaruppan, M.C.; Vezhavendhan, R.; Chandramohan, P.; Rathinasabapathi, G. Impact of novel clay dispersion on mechanical, thermal, and vibration properties of IPN composites. *Polym. Compos.* **2024**, *45*, 16882–16897. [CrossRef]
46. Riaz, S.; Rehman, A.U.; Akhter, Z.; Najam, T.; Hossain, I.; Karim, R.; Assiri, M.A.; Shah, S.S.A.; Nazir, M.A. Recent advancement in synthesis and applications of LDH composites. *Mater. Today Sustain.* **2024**, *27*, 100897. [CrossRef]
47. Keyikoğlu, R.; Khataee, A. LDHs as sustainable catalysts in electrocatalytic water treatment. *J. Environ. Chem. Eng.* **2025**, *13*, 115275. [CrossRef]
48. Coiai, S.; Passaglia, E.; Telleschi, A.; Oberhauser, W.; Coltelli, M.-B.; Cicogna, F. A sustainable multistage process for immobilizing bioactive compounds on LDHs. *Cosmetics* **2024**, *11*, 52. [CrossRef]
49. Huang, J.; Xu, B.; So, M.Y.; Liu, X.; Gao, Y. A hierarchical LDH electrode with porous fibers. *J. Mater. Chem. A* **2024**, *12*, 7187–7198. [CrossRef]
50. Wong, M.-K.; Loh, J.Y.; Yap, F.M.; Ong, W.-J. Fueling clean energy with LDH-based electrocatalysts. *InfoMat* **2025**, *7*, 2. [CrossRef]
51. Mestry, J.; Abdelwahab, M.A.; Elkholy, H.M.; Rabnawaz, M. Mechanical Recycling of a Bottle-Grade and Thermoform-Grade PET Mixture Enabled by Glycidol-Free Chain Extenders. *Ind. Eng. Chem. Res.* **2024**, *63*, 18067–18074. [CrossRef]
52. Shirazimoghaddam, S.; Amin, I.; Albanese, J.A.F.; Shiju, N.R. Chemical recycling of PET by glycolysis using niobia catalysts. *ACS Eng. Au* **2023**, *3*, 37–44. [CrossRef]

53. Jo, Y.; Kim, E.J.; Kim, J.; An, K. Efficient Fe_3O_4 nanoparticle catalysts for PET depolymerization. *Green Chem.* **2023**, *25*, 8160–8171. [CrossRef]
54. Wang, Z.; Shi, J.; Jin, Y.; Xiao, G.; Su, H. Recyclable zinc cyanamide dual-site catalyst for PET glycolysis. *ACS Appl. Polym. Mater.* **2025**, *7*, 1609–1617. [CrossRef]
55. Mohan, M.; Keasling, J.D.; Simmons, B.A.; Singh, S. COSMO-RS screening of ionic liquids for plastic dissolution. *Green Chem.* **2022**, *24*, 4140–4152. [CrossRef]
56. Wang, R.; Wang, T.; Yu, G.; Chen, X. Deep eutectic solvent@ZIF-8 catalyst for PET glycolysis. *Polym. Degrad. Stab.* **2021**, *183*, 109463. [CrossRef]
57. Wang, Z.; Jin, Y.; Wang, Y.; Tang, Z.; Wang, S.; Xiao, G.; Su, H. Cyanamide as an efficient organocatalyst for PET glycolysis. *ACS Sustain. Chem. Eng.* **2022**, *10*, 7965–7973. [CrossRef]
58. Delle Chiaie, K.R.; McMahon, F.R.; Williams, E.J.; Price, M.J.; Dove, A.P. Dual-catalytic depolymerization of PET. *Polym. Chem.* **2020**, *11*, 1450–1453. [CrossRef]
59. Wang, L.; Nelson, G.A.; Toland, J.; Holbrey, J.D. Glycolysis of PET using imidazolium-carboxylate organocatalyst. *ACS Sustain. Chem. Eng.* **2020**, *8*, 13362–13368. [CrossRef]
60. Chiao, Y.-W.; Liao, W.; Krisbiantoro, P.A.; Yu, B.-Y.; Wu, K.C. Waste-battery-derived zinc catalysts for PET glycolysis. *Appl. Catal. B Environ.* **2023**, *325*, 122302. [CrossRef]
61. Lin, Y.; Yang, D.; Meng, C.; Si, C.; Zhang, Q.; Zeng, G.; Jiang, W. Monatomic oxygen anion generation over Ni^{2+}-doped MgO for PET glycolysis. *ChemSusChem* **2023**, *16*, e202300154. [CrossRef]
62. Li, Y.; Shen, J.; Liu, Q.; Zhu, Y.; Pang, Z.; Ge, M. Zinc-doped ferrite nanoparticles as bifunctional catalysts for PET fabric glycolysis. *J. Environ. Chem. Eng.* **2023**, *11*, 109816. [CrossRef]
63. Eshaq, G.H.; El-Metwally, A.E. (Mg–Zn)–Al LDH as a regenerable catalyst for PET glycolysis. *J. Mol. Liq.* **2016**, *214*, 1–6. [CrossRef]
64. Zhang, F.; Xiang, X.; Li, F.; Duan, X. Layered double hydroxides as catalytic materials. *Catal. Surv. Asia* **2008**, *12*, 253–265. [CrossRef]
65. Debecker, D.P.; Gaigneaux, E.M.; Busca, G. Exploring the basicity of hydrotalcites for heterogeneous catalysis. *Chem. Eur. J.* **2009**, *15*, 3920–3935. [CrossRef]
66. Soni, S.; Kumari, A.; Sharma, A.; Bhatia, S.K.; Sharma, A. Tetravalent metals modulated Zn-based layered double hydroxides and their mixed metal oxides for catalytic depolymerization of carbonyl-coordinating plastic waste. *Catal. Today* **2025**, *446*, 115136. [CrossRef]
67. Da Silva, T.S.; da Silva, L.L.F.F.; da Silva, E.P.S.; Motta, R.J.B.; da Silva, B.J.B.; Meneghetti, M.R.; Meili, L.; Meneghetti, S.M.P. From Waste to Catalyst: The Properties of Mixed Oxides Derived from Layered Double Hydroxide Mg/Al Synthesized from Aluminum Residues and Their Use in Transesterification. *Reactions* **2025**, *6*, 33. [CrossRef]
68. Soni, S.; Kumari, A.; Sharma, A.; Jaswal, V.S.; Bhatia, S.K.; Sharma, A.K. MAl-X [M-Zn, Mg, Ni; X- Cl, NO_3, CO_3] layered double hydroxides: Catalytic applicability in plastic waste recycling and wastewater treatment for the sustainable environment. *Emergent Mater.* **2025**, *8*, 2505–2524. [CrossRef]
69. Kumari, S.; Soni, S.; Sharma, A.; Sharma, V.; Sharma, A.K. MAl-CO_3-based layered double hydroxides for catalytic depolymerization of poly(ethylene terephthalate) and poly(bisphenol A carbonate) waste materials. *Appl. Catal. O Open* **2024**, *189*, 206922. [CrossRef]
70. Martínez-Vila, S.; Riera-Malgosa, L.; Prieto-Fuentes, R.; Duran-Serra, A.; Carrillo-Navarrete, F. Chemical recycling of polyester fabrics by alkaline hydrolysis using alcohols as cosolvents. *Sustain. Chem. Pharm.* **2025**, *43*, 101891. [CrossRef]
71. Slezák, E.; Ronkay, F.; Bocz, K. Development of engineering material with enhanced impact strength and heat resistance from recycled PET. *J. Polym. Environ.* **2023**, *31*, 5296–5308. [CrossRef]
72. Fiorillo, C.; Trossaert, L.; Bezeraj, E.; Debrie, S.; Ohnmacht, H.; Van Steenberge, P.H.; Edeleva, M. Molecular and material property variations during ideal degradation and mechanical recycling of PET. *RSC Sustain.* **2024**, *2*, 3596–3637. [CrossRef]
73. Gao, M.; Jiao, Q.; Cui, W.; Feng, C.; Zhao, Y.; Xiang, A.; Mu, X.; Ma, L. Preparation of PET/LDH composite materials and their mechanical properties and permeability for O_2. *Polym. Eng. Sci.* **2019**, *59*, E366–E371. [CrossRef]

Disclaimer/Publisher's Note: The statements, opinions and data contained in all publications are solely those of the individual author(s) and contributor(s) and not of MDPI and/or the editor(s). MDPI and/or the editor(s) disclaim responsibility for any injury to people or property resulting from any ideas, methods, instructions or products referred to in the content.